Ming Xu · Xiaoyue Yu · Yuhua Pan · Xianshan Liu · Yuanping Zhao · Jiaju Hu

Analysis of the seismic dynamic response and failure mode of the Layue landslide

Abstract Shear failure of bedding slopes along weak zones is the main failure mechanism of the Layue landslide. To investigate the seismic dynamic response and destabilization failure mode of rock slopes with laminated fracture structures, a two-dimensional shaking table test with different ground motion inputs was performed, taking into consideration a variety of factors, such as the input seismic wave type and amplitude. The results show that the ground shaking characteristics and geological structure of the slope are the decisive factors in determining the seismic dynamic stability and failure mode of the slope. The horizontal dynamic response of the slope has an obvious elevation amplification effect and topographic effect, and the elevation has less influence on the vertical dynamic response of the slope. The ground motion amplification effect is related to the mechanical strength of the structural surface, the waveform of seismic waves, and the spectral characteristics. The sine wave has a more significant influence on the amplification effect of the slope than the natural wave. The slope cracks are initiated and propagate at the weakest part depending on the dominant structural surface and trace to the joint surface to form creep sections and locking sections. The strength parameter of the joint surface weakens under the action of geological agents, which results in two failure modes of the slope: the forward failure mode and the backward failure mode. The former refers to the potential slip belt lap through from the trailing edge to the front edge, where the sliding mass is cut out from the high position. The latter refers to the potential slip belt lap through the front edge to the trailing edge, and the sliding mass breaks down and is destroyed. Through a unique adaptive device, the seismic anchor cable can coordinate the deformation of the anchor cable with the rock-soil body, which can reduce the risk of a slope earthquake disaster.

Keywords Bedding rock slope · Block model · Shaking table test · Seismic ground motion parameters · Dynamic response · Failure mode

Introduction

Earthquakes have a triggering effect on the instability of geotechnical slopes, which often induces numerous secondary collapses and landslide disasters. This effect poses a great hidden danger to urbanization construction due to potential major casualties and property losses (Yin et al. 2009). The geological disasters triggered by earthquakes show a series of characteristics different from those in a gravity environment, such as the unique instability mechanism (Eberhardt et al. 2004; Gischig et al. 2015a, b; Hovius and Meunier 2012), large-scale high-speed projectiles (Sassa et al. 2010), super dynamic characteristics, and long-distance movement (Deng et al. 2017; Zhang et al. 2011), mountain cracking and loosening, and vast landslides blocking rivers (Zhou et al. 2013; Chen et al. 2011). These

phenomena and problems far exceed the categories of the original cognition and knowledge of most people (Huang and Li 2009; Huang et al. 2011).

Laminated slopes are common geological bodies in the southwest mountains of China, with significant regional characteristics. Many scholars have studied the dynamic response characteristics and deformation mechanisms of laminated slopes using physical tests, numerical simulations, and analytical calculations. He et al. revealed the progressive failure characteristics and four stages of the layered slope by using a large-scale shaking table test (He et al. 2021). Xu et al. conducted the law of dynamic characteristics and dynamic response under seismic action and the influences of ground motion parameters on the dynamic characteristics and dynamic response (Xu et al. 2008). Liu et al. researched the dynamic response processes of the horizontal weak interbedded rock slopes with different thicknesses under earthquake action (Liu et al. 2021a). Dong et al. studied the acceleration, displacement, acoustic emission, and failure mode of bedding rock slopes under earthquakes by large-scale shaking table tests (Dong et al. 2022). Ye et al. used seismic waves with different parameters to study the dynamic response of local blocks at the top of the slopes under seismic action and the projectile phenomenon of sliding bodies at the top of the slope (Ye et al. 2012). Fan et al. studied the seismic dynamic response of consequent slopes and reverse slopes (Fan et al. 2016). Li et al. studied the slope particle flow behavior and related sedimentary characteristics through a series of flume tests under different particle size and volume conditions (Li et al. 2021).

At present, many research achievements have been made to the seismic response of layered rock slopes (Yang et al. 2018; Liu et al. 2013, 2021b). However, most of the shaking table slope models are modulated by a variety of materials according to a certain mix ratio (Feng et al. 2019; Liang et al. 2005; Tao et al. 2021), and this method has difficulty reflecting the particularity and complexity of slope structures cut by interlaminar joints and secondary joints. In addition, the dynamic response characteristics of the layered slope are difficult to fully understand due to the discontinuity of the structural plane distribution and geological material in the layered slope, as well as the complex mechanism of the structural plane and seismic wave (Huang et al. 2017). In particular, the damage mechanism and the gradual damage degradation, deformation accumulation, and landslide breeding of slope geotechnical materials and structures under long-term internal and external dynamic geological action of slopes are insufficiently studied; meanwhile, there is no systematic comparative analysis of the activity characteristics and stability changes of layered cataclastic rock slopes.

In this paper, a block masonry slope shaking table model is used to legitimately characterize the rock mass structure characteristics of

layered cataclastic rock slopes. Under the action of two-dimensional and multiparameter ground motion, shaking table physical model tests of the slope were carried out with three kinds of gradual mechanical strength. The influences of ground motion parameters and rock structure parameters on the slope dynamic response and failure mode were studied.

Profile of prototype slope

Layered cataclastic rock slopes are mostly controlled by complex geological structures such as folds and faults. The interlayer joints and secondary joints are extremely well developed, and the lithology is mostly hard rock, the stability of which is closely related to the geological environment. For example, the layered fractured mosaic structure presented by the Mount Emei basalt geomorphic unit is formed by the superposition of structural fissures and columnar joints produced by the folding movement. The plain view drawing and geological profile of the Layue landslide are shown in Fig. 1.

The Layue landslide is a typical downdip stratiform dramatic landslide, located on the left bank of the Layue Qu of the Tongmai-Pailong section of the Sichuan-Tibet Highway, with an average slope of more than 45°. It is mainly composed of exposed granitic gneiss and rhyolite granite, with lamellar structures, formed by the directional arrangement of dark minerals in the rocks under tectonic action. Under the influence of tectonic activity, joints and fissures are well developed in the rock mass, and the maximum stress direction is north–south extrusion, forming massive rock mass block structures with different characteristics. The attitude of similar bedding is $170 \sim 180° \angle 30 \sim 40°$, and the dip is nearly consistent with the aspect. The conjugate development "X"-type joint obliquely intersects the slope side, with the occurrence of $60 \sim 70° \angle 60 \sim 65°$ and $340 \sim 345° \angle 64 \sim 76°$. The integrity of the rock mass is poor under the joint cutting of discontinuous surfaces such as bedding and joints, and it is mostly a layered cataclastic or blocky structure. The combination of the layered structure along the slope and the free face with a steep top and gentle bottom creates the foundation and boundary conditions for the fractured bedrock to slip out of the slope.

Due to the impact of tectonic movement, this area has been strongly uplifted since the Cenozoic, and seismic activity is very frequent. The stability of the Layue landslide decreased due to the effects of the earthquake on August 15, 1950. Then, the slope body deformed slowly under the action of dead weight, many obvious cracks appeared with slow development, and collapses of varying sizes occurred frequently. In late July 1962, five earthquakes of Ms = 4.5–4.7 occurred in succession, which led to the deepening and widening of the surface cracks of the Layue landslide and intensified slope deformation and destruction. The frequency of small collapses and landslides increased obviously. Moreover, 1962 was a wet year in the Parlung Zangbo Basin. Rainwater and groundwater infiltrated the cracks, and under the influences of dynamic and hydrostatic pressure and the soaking softening effect on weak interlayers in bedrock, sliding discontinuities in the weathering crust of bedrock and rock mass became possible. After 5 years of development, the Layue landslide occurred on August 29, 1967. The back scarp was an armchair bedrock escarpment with a slope of 60–70° and an elevation of 2700–2800 m. The average length of the sliding mass was 450 m, the average width was 500 m, and the average thickness was approximately 50 m. The sloped body was cut out from the high position in the middle of the slope with a relative height difference of $400 \sim 700$ m. The sliding surface was steep-shaped, the main sliding direction was approximately 159°, and the volume was more than ten million cubic meters. The sliding mass was distributed in the main sliding zone of the landslide at $2450 \sim 2650$ m and its lower landslide accumulation zone.

Design of the shaking table test scheme

Similarity condition design

Rock mass structure is one of the main controlling factors of slope stability; thus, the model must be established according to the rock mass structure of the prototype. According to the similarity theory and the purpose of model test research, in the model test of the Layue landslide, the similarity of rock mass structure and mechanical (including dynamic) characteristics was mainly adopted as the basic condition. The similarity of the model material, structure, stress mode, and failure mode were given priority, followed by the size and proportion of the model. Therefore, density ρ, elastic modulus E, and acceleration a were taken as control quantities of similar design in the model test. Other physical quantities related to slope deformation
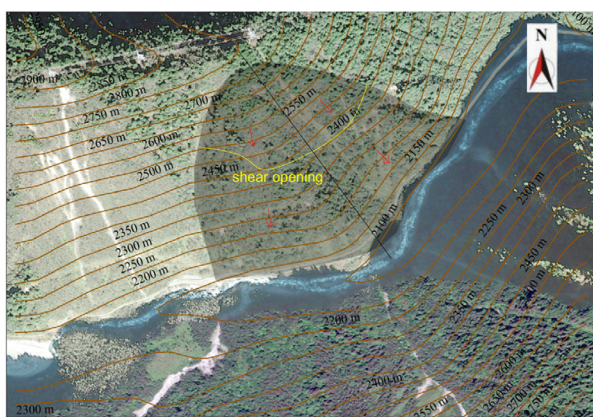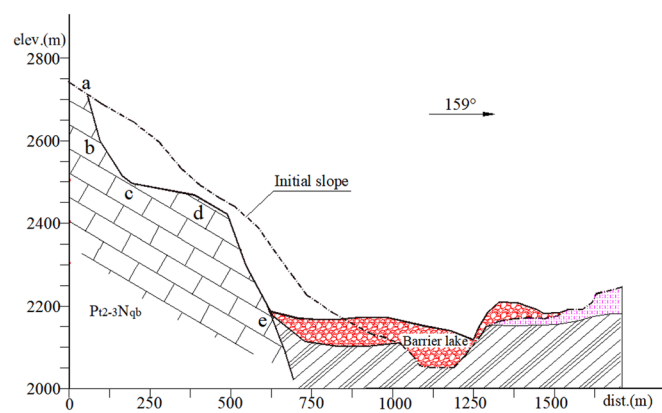
Fig. 1 Layue landslide: **a** plain view drawing; **b** geological profile

Table 1 Similarity coefficients of shaking table modeling

Parameter type	Physical quantities	Dimension	Similarity coefficient formula	Similarity factor	
				Theoretical	Actual
Material parameters	Density ρ[a]	ML^{-3}	C_ρ	1	0.99
	Elastic modulus E[a]	$ML^{-1}T^{-2}$	C_E	100	0.95
	Cohesion c	$ML^{-1}T^{-2}$	$C_c = C_E$	100	1
	Internal friction angle φ	–	$C_\varphi = 1$	1	0.96
	Stress σ	$ML^{-1}T^{-2}$	$C_\sigma = C_E$	100	–
	Strain ε	–	$C_\varepsilon = 1$	1	1
	Poisson's ratio μ	1	$C_\mu = 1$	1	1
Geometric parameters	Displacement u	L	$C_u = C_\rho^{-1}C_E C_a^{-1}$	100	1000
	Length l	L	$C_l = C_\rho^{-1}C_E C_a^{-1}$	100	1000
Kinematics parameters	Acceleration a[a]	LT^{-2}	C_a	1	$0.3\sim3$
	Time t	T	$C_t = C_\rho^{-\frac{1}{2}}C_E^{\frac{1}{2}}$	10	10[b]
	Frequency f	T^{-1}	$C_f = C_\rho^{\frac{1}{2}}C_E^{-\frac{1}{2}}C_a$	0.1	0.1[b]
	Speed v	LT^{-1}	$C_v = C_\rho^{-\frac{1}{2}}C_E^{\frac{1}{2}}$	10	10[b]
	Acceleration g	LT^{-2}	$C_g = C_a$	1	1
	Damping ratio ξ	–	$C_\xi = 1$	1	1

[a]represents control quantity, and [b]represents moderate relaxation

were kept as similar as possible. The similarity constants of each physical quantity in the model test are shown in Table 1.

Model design

The rock type of the Layue landslide is mainly mélange and is strongly impacted by tectonic activity. The rock mass is divided into different blocks by different joints and similar bedding, and the combination of different blocks constitutes the rock mass structure of the slope. Rock mechanics and physical parameters of landslides are shown in Table 2. In this paper, natural stone was selected as the landslide block after cutting and polishing. The block size is 30*30*200 mm, and the length–width ratio reflected the different intensive degrees of the development of "X"-type joints at the oblique intersection with the slope. The physical and mechanical tests of the rock are shown in Fig. 2.

The physical and mechanical parameters of the test blocks were obtained by using a WADJ-600 type microcomputer-controlled electrohydraulic servo rock shear rheological testing machine according to the uniaxial compression test and direct shear test, as shown in Table 2.

The model structural surface considered three groups of joints (Table 3), such as the bedding along the slope and conjugate "X"-type joints intersecting diagonally with the slope, which exert the greatest influence on the stability of the slope. The strip-shaped blocks were stacked in parallel with a dip angle of 30° to form a lamellar structure along the slope. The joint plane was obliquely intersected with the slope, and the dip angle was 60°.

The rock body in the area of Layue was affected by complex tectonic stress and seismic activity for a long time, and the structure was fragmented. The mechanical parameters of the sliding surface are time-dependent and spatially variable with the development

Table 2 Physical and mechanical parameters of slope rock

Category	Gravity γ/kN·m^{-3}	Cohesion c/kPa	Internal friction angle φ/°	Compressive strength σ_c/MPa	Elastic modulus E/GPa	Poisson's ratio μ
Slider	26.2	690	39.3	24.2	29.13	0.2
Blocks	26.4	1950	41	21.4	30.8	0.2
Sliding surface		$10\sim100$	$15\sim50$			

Fig. 2 Rock physical and mechanical parameters test

of the geological structure, stratum structure, earthquakes, and climate. To reasonably determine the strength parameters of the potential slip surface, the c and φ values of the slip zone were calculated by finite element back analysis. The suggested values for the model experimental interlayer joints were proposed by comprehensive analysis of the inverse algorithm, experimental values, and empirical values, as shown in Table 4.

Under seismic loading, the failure evolution mode of rock slopes is simulated by the field-enriched finite element method (Wang and Zhou 2021; Zhou et al. 2021). Based on the variational principle, the force balance equation of the damaged material was derived. Apart from the displacement field, an additional degree of freedom was introduced at each element node, namely, the damage field. The stiffness in the constitutive model was attenuated by the degradation function, which was equivalent to discrete cracks, thus affecting the displacement field distribution.

$$g(d) = (1 - d)^2 \qquad (1)$$

defined the slope stiffness attenuation function $g(d)$. d is the damage variable interpolated between damaged ($d=1$) and undamaged ($d=0$) materials. This function was used to attenuate elastic strain energy, which was closely related to the current damage state, and was selected in the form of a quadratic polynomial.

The distribution of the damage field adopted the exponential distance weighting method, which could constrain the crack within a narrow band, and its distribution function could be expressed as:

$$d(s) = e^{-s/l} \qquad (2)$$

where d is the damage field, s is the distance to the crack, and l is the control factor for the extent of the enriched crack.

The J-integral of the crack tip was solved by the displacement field, stress field, and fracture mechanics method to obtain the stress intensity factor. According to the crack extension criterion, the crack extension direction and extension increment was determined. The cracks further competed for evolution and divided the slope into through planes with different development degrees. This method could reveal the evolution process of potential fractures (shearing section) and rock bridges (locking section) on the slip surface and the progressive degradation of the mechanical parameters of the landslide.

Model 1 was taken as a comparison specimen, and no damage occurred during the static and dynamic tests. Models 2 and 3 describe the damage evolution of the slope under earthquake and rainfall conditions through the degradation of shear parameters of the slip zone to different degrees.

Cementing materials with different cohesive strengths were used to simulate the attenuation and degradation of the mechanical parameters of the fracture surface. The cementing material was prepared by mixing water, medium-coarse sand, gypsum, and glycerin according to the mass ratios of 40:100:0:5, 40:100:7.5:5, 40:100:15:5, and 40:100:20:5. Medium-coarse sand played the role of aggregate, gypsum had the effect of cementation, and glycerin enabled water retention. The parameters of the cementing material are shown in Table 4.

The cementing materials with different cohesive strengths were combined in pairs and used to represent different cohesion and internal friction angles of the interlayer joint along the slope direction and secondary joint against the slope direction, respectively, thus forming three groups of specimens. As shown in Fig. 3a, in model 1, the red part represents the secondary joint cemented by ultrahigh-strength material A, and the black part represents the interlaminar joint cemented by high-strength material B. A1–A4 are the monitoring points of the acceleration sensor. In Fig. 3b, model 2 is cemented by material B and material C. Compared with model 1, the cohesion of interlaminar joints in model 2 decreased by 40% along the slope, and the internal friction angle decreased by 52%. In Fig. 3c, model 3 is cemented by material C and material D. Compared with model 2, the cohesion of interlaminar joints in model 3 decreased by 70% along the slope, and the internal friction angle decreased by 39%. The interlayer joints of the same lithology in the same area were more developed than the secondary joints, and their shear strength was weaker than that of the secondary joints, which reflected the real mechanical condition of the joint and fissure of the prototype slope.

Table 3 Comparison of the structural plane between prototype and model slope

Number	Prototype structure surface	Characteristic	Model structure surface	Characteristic
1	175°∠35°	Stratification	Down-slope structural surface, inclination angle 30°	Bedding
2	65°∠60°	Joint occurring co-choked in the region	Reverse slope structural surface, inclination angle 60°	Reverse slope direction
3	345°∠70°			Oblique slope intersection

Table 4 Parameters of cementing material

Cementing material code	Mixing ratio (mass ratio) (water:coarse sand:gypsum:glycerin)	Work conditions	Cohesion c/kPa	Internal friction angle φ/°
A	40:100:20:5	Static (joint)	86	57
B	40:100:15:5	Static (stratification)	62	48
C	40:100:7.5:5	Earthquake	37	23
D	40:100:0:5	Earthquake + rainfall	11	14

Sensor arrangement

The American ANCO Engineers R-100HV small seismic simulation shaking table test system was adopted for this experimentation. The table size was 1.2 m*1.2 m, the maximum load capacity was 1000 kg, and the working frequency was 0–50 Hz. The table can vibrate horizontally and vertically at the same time.

The length, width, and height of the model box were 0.55*0.5*0.6 m, respectively. A 2-cm-thick layer of gravel and medium (coarse) sand was laid between the bottom of the model box and the slope model, to limit the bottom boundary distortion caused by sliding of the slope model during vibration. A 2-cm-thick polystyrene plastic foam board was pasted on the sidewall of the model box, to reduce the friction between the sidewalls and the impact of seismic wave reflection on the boundary.

Acceleration nodes were set at the top, surface, and foot of the slope. Two measuring points were arranged at the shear outlet elevation in the middle of the slope. A total of 4 groups of JM5840 three-direction wireless acceleration sensor nodes were set, and the acquisition frequency was 512 Hz. The online monitoring system was constructed by the JM1803 wireless gateway and JMTEST dynamic signal testing and analysis software. A Huagu Power WP-UT500 high-speed camera was arranged to collect landslide motion video signals from the front and side of the slope model, as shown in Fig. 4.

Test loading scheme

The input seismic waves included the Sine wave, Taft wave, El-Centro wave, and Wolong wave. Before loading the natural wave, baseline correction and filtering were carried out on the original waveform, and compression was carried out according to the time similarity ratio with a loading holding time of 5 s, as shown in Fig. 5.

The Fourier transform of the three natural waves was carried out to obtain their remarkable frequencies between 15 and 25 Hz, and the sine wave frequencies were set to four kinds 6, 8, 10, and 12 Hz. The loading scheme was set in five groups, and the first four loading schemes corresponded to four amplitudes of 0.1, 0.2, 0.3, and 0.4 g. Each group was set in three excitation directions: horizontal vibration, vertical vibration, and combined vibration, where the frequencies of the two waveforms of horizontal and vertical vibration were set to 8 Hz. However, the waveforms of combined vibration were set in four frequencies from 6 to 12 Hz, and the amplitude of the vertical direction was 2/3 of that of the horizontal direction. The input waveform loading scheme is shown in Table 5, and all three models used the same seismic waveform loading conditions.

Analysis of test results

The peak ground acceleration (PGA) amplification factor was defined as the ratio of the peak values of horizontal and vertical accelerations between the slope monitoring points and the input
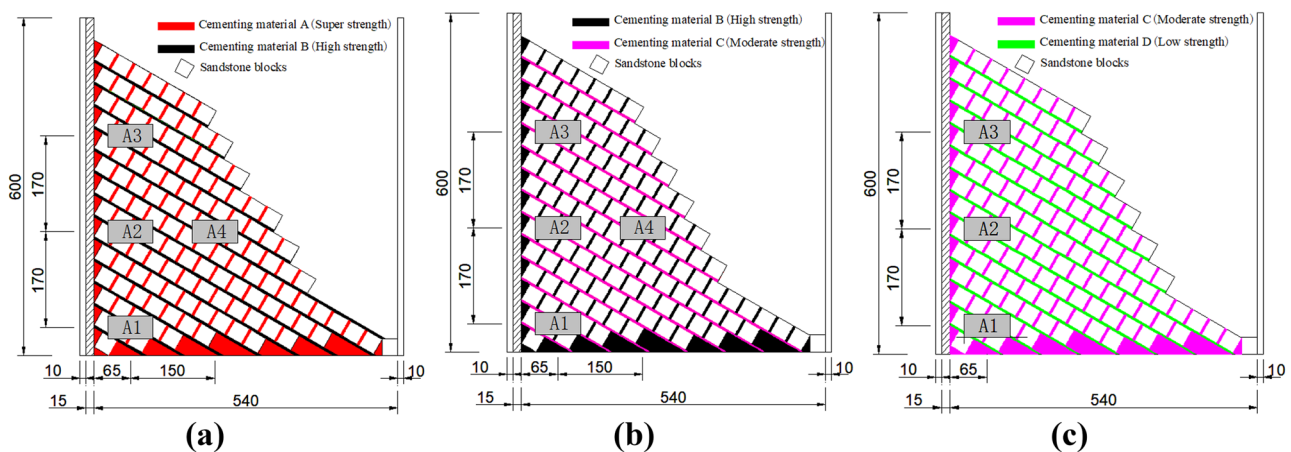
Fig. 3 Model specimen (unit:mm): **a** model 1; **b** model 2; **c** model 3
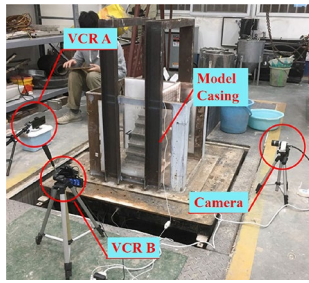
Fig. 4 Site layout of shaking table test equipment

seismic waves. The differences in the seismic dynamic responses of the three groups of slopes were analyzed by comparing the amplification coefficients.

Horizontal acceleration dynamic response

Figure 6 shows the variation pattern of the horizontal PGA amplification coefficient with seismic wave type at monitoring point A2 in model 1 under different amplitudes. The 8-Hz sine wave is selected for the comparative analysis. The horizontal PGA amplification coefficient increases in the order of Wolong wave, El wave, Taft wave, and sine wave because the spectrum characteristics of different types of seismic waves are different. The three natural waves increase through relatively small intervals. The fundamental frequency of the Wolong wave is larger than the natural vibration frequency of the slope structure, so the dynamic response of the slope is small and the horizontal PGA amplification coefficient is low. The frequency of the sine wave is close to the natural vibration

frequency of the slope structure, so the amplification effect of the horizontal acceleration of the slope is very obvious.

The corresponding elevations of monitoring points A1, A2, and A3 were defined as elevation 1, elevation 2, and elevation 3, respectively. Under the excitation of an 8-Hz sine wave, the horizontal PGA amplification coefficient decreases first and then increases with the seismic amplitude, as shown in Fig. 7. In the lower amplitude range of the seismic wave (less than 0.3 g), with the increase in the amplitude of the input wave, the slope dynamic response and the PGA amplification coefficient decrease. This is because with the accumulation of seismic action, the low-order natural frequency of the model slope decreases, while the damping ratio gradually increases, and the model slope exhibits obvious nonlinear characteristics. When the amplitude exceeds 0.3 g, the amplification coefficient increases with the increase in the amplitude of the input wave, but its rates of increase gradually decline. The degree of this effect should be related to the rock structure; alternatively, the rock mass structure controls the natural vibration characteristics of the rock mass according to a certain law. The reason for this phenomenon can be explained by the increase in the amplitude, the accumulated damage, the obvious nonlinear characteristics, the decrease in the high-order natural frequency of the structure, and the decrease in the gap with the input frequency. At different amplitudes, the horizontal PGA amplification coefficient of the slope shows a nonlinear increasing trend with increasing elevation, which exhibits an obvious elevation amplification effect (Wang et al. 2018). Therefore, the most significant dynamic response occurs at the shoulder of the slope, which is often the origin of earthquake damage accumulation and crack propagation.

Figure 8 shows the acceleration amplification coefficients of the A2 and A4 monitoring points at the same elevation under the action of 8-Hz sine waves with different amplitudes. The amplification effect of A4 on the slope is always greater than that of A2 on the slope, showing an obvious topographic effect.
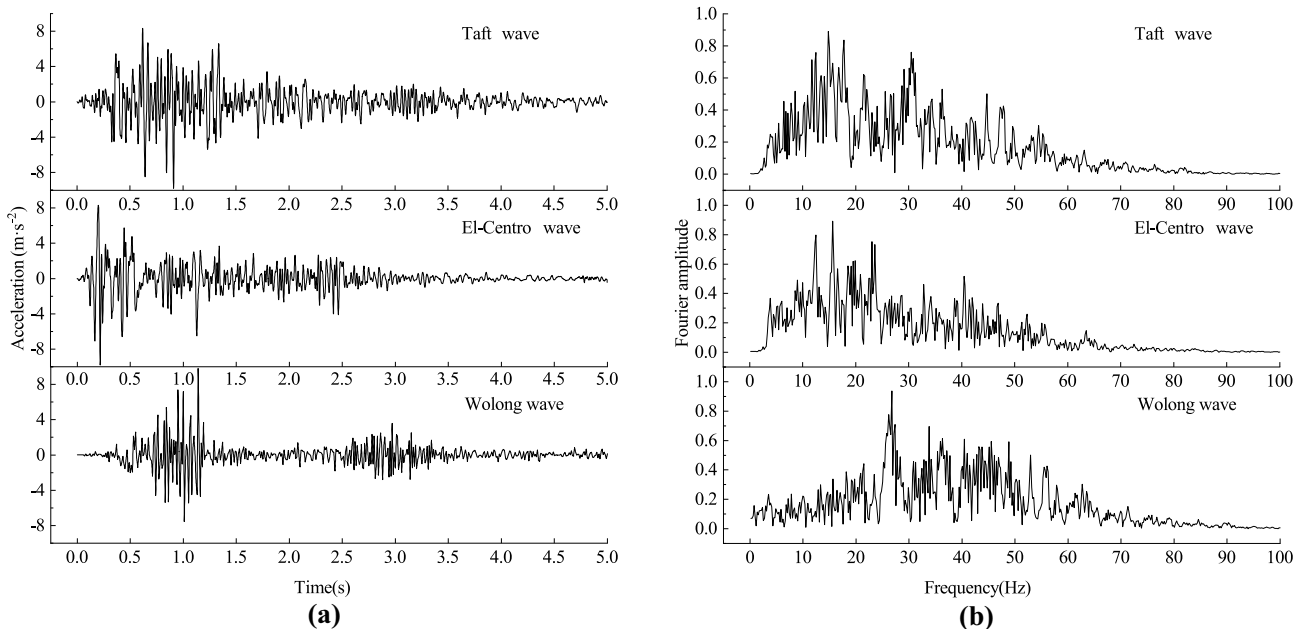

Fig. 5 Time history curve of acceleration and Fourier spectrum of natural seismic wave: **a** acceleration time curve; **b** Fourier spectrum

**Table 5** Loading condition table of the input wave

Work condition serial number	Seismic wave type	Amplitude/g	Frequency/Hz	Duration/s	Magnitude grouping
1	White noise	H:0.05 + V:0.05		5	Group 1 work conditions 1 ~ 10
2	Sine wave	H:0.1	8	5	
3	Sine wave	V:0.067	8	5	
4 ~ 7	Sine wave	H:0.1 + V:0.067	6 ~ 12	5	
8	El wave			5	
9	Taft wave			5	
10	Wolong wave			5	
11 ~ 30	…	…	…	…	Group 2 ~ 3
31	White noise	H:0.05 + V:0.05		5	Group 4 work conditions 31 ~ 40
32	Sine wave	H:0.4	8	5	
33	Sine wave	V:0.267	8	5	
34 ~ 37	Sine wave	H:0.4 + V:0.267	6 ~ 12	5	
38	El wave			5	
39	Taft wave			5	
40	Wolong wave			5	
41	White noise	H:0.05 + V:0.05		5	Group 5 work conditions 41 ~ 47
42 ~ 47	Sine wave	H:0.5 + V:0.333 ~ H:1 + V:0.677	8	5	

Figure 9 shows the variation pattern of the horizontal PGA amplification coefficient with the peak acceleration, at the monitoring point A2 of the three groups of model slopes. When the peak acceleration of the input ground motion is less than 0.3 g, the amplification coefficient of the horizontal PGA increases with the weakening of mechanical properties of the bedding and joints, and

the rate of increase is enhanced with the amplitude of the input wave. When the peak acceleration of the input ground motion is greater than 0.3 g, the amplification coefficient of the horizontal PGA decreases with the weakening of mechanical properties of the bedding and joints, and the amplitude of the reduction increases with the amplitude of the input wave.
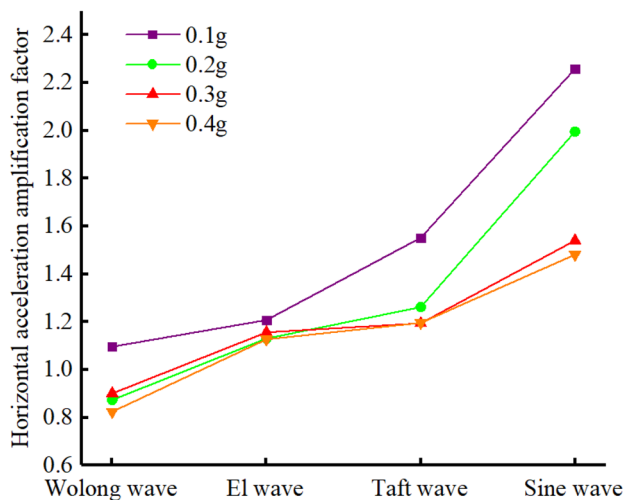
Fig. 6 The effect of seismic wave type on horizontal PGA amplification coefficient
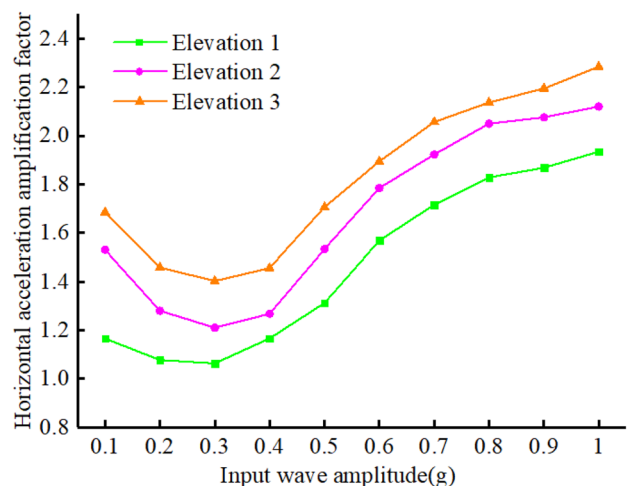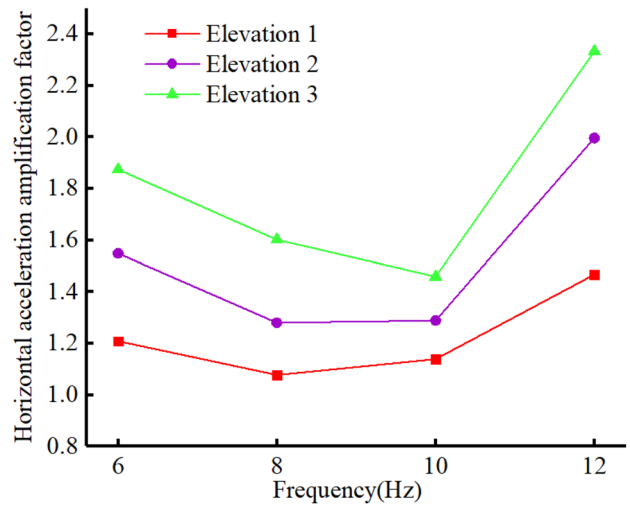

Fig. 7 Influence of slope elevation and seismic amplitude on horizontal PGA amplification coefficient
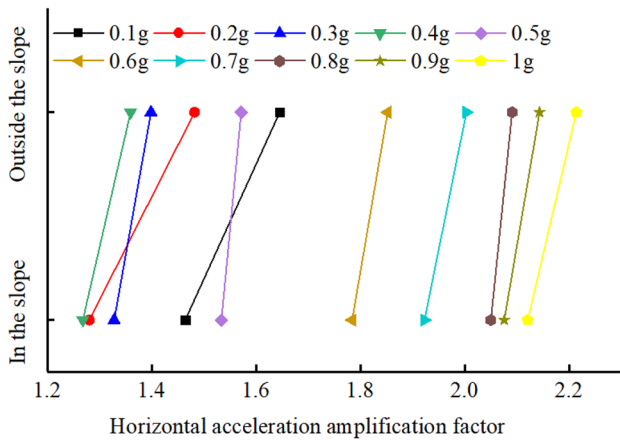
Fig. 8 Effect of horizontal position on horizontal PGA amplification factor

Fig. 10 Influence of seismic wave frequency on horizontal PGA amplification coefficient

As shown in Fig. 10, when the seismic wave amplitude is 0.2 g, the influence of the input wave frequency on the horizontal PGA amplification coefficient shows a characteristic of initial depression and subsequent increase. The slope has multi-order natural frequencies, and formants are formed at multi-order frequency points. The amplification coefficient of the horizontal PGA decreases gradually in the nonresonant region (6–10 Hz). When the frequency exceeds 10 Hz, the amplification coefficient increases significantly. This shows that the rock mass structure has a great influence on the rock mass resonance, but in the range of non-resonant frequencies, the rock mass structure has little influence on the vibration response value of the fractured rock mass. The seismic response of the slope is related not only to the characteristics of the slope structure itself but also to the waveform, spectral characteristics, and duration of the seismic wave.
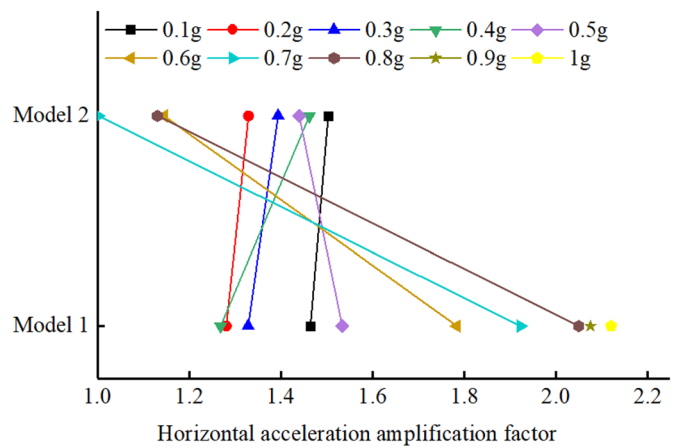
Vertical acceleration dynamic response

Figure 11 shows the variation pattern of the vertical PGA amplification coefficient with slope elevation when the peak acceleration of input ground motion in model 1 is 0.3 g. The influence of elevation on the vertical acceleration amplification factor is nearly zero, while the influence of the seismic wave type is substantial. The amplification effect of the sine wave on the vertical acceleration of the slope is very obvious, followed by the El wave, Wolong wave, and Taft wave. This is slightly different from the case for the horizontal PGA amplification coefficient, indicating the influence of the anisotropy of the rock mass structure on the horizontal and vertical formants.
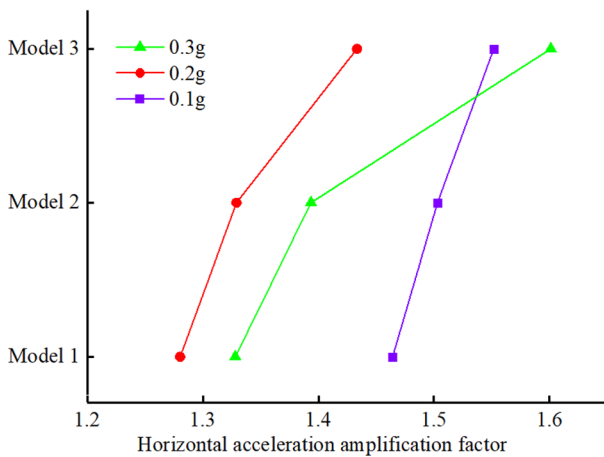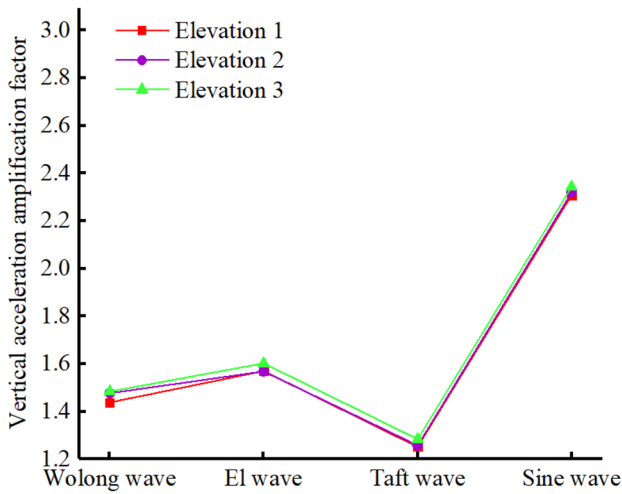

(a)

(b)

Fig. 9 Horizontal PGA amplification coefficient of monitoring points in the middle of the slope: **a** peak acceleration of ground motion 0.1 ~ 0.3 g; **b** peak acceleration of ground motion 0.1 ~ 1 g
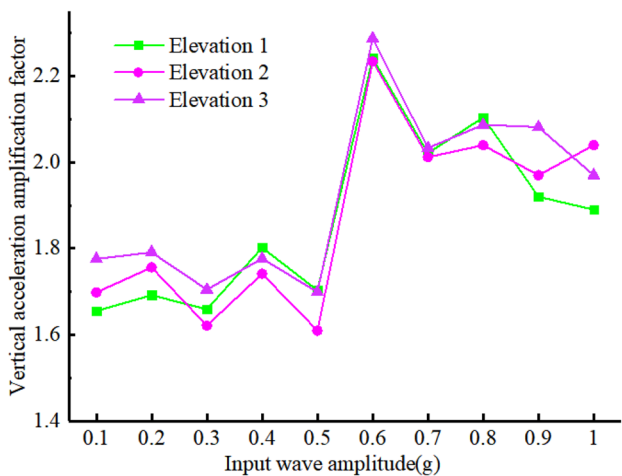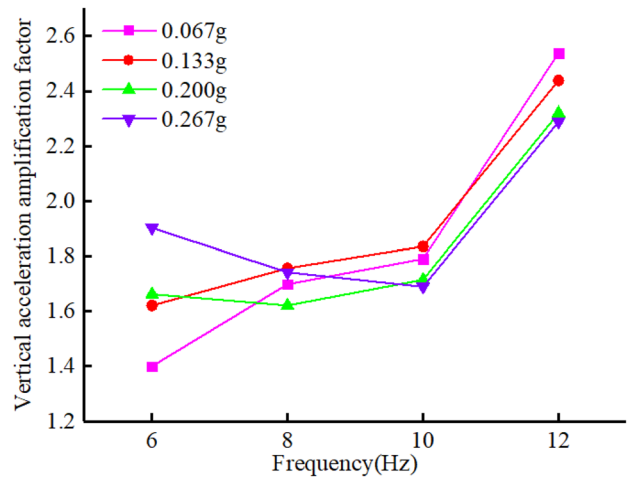
Fig. 11 Effect of seismic wave type on vertical PGA amplification coefficients at different elevations

Fig. 13 Influence of seismic wave frequency on vertical PGA amplification coefficient

Figure 12 shows the variation pattern of the vertical PGA amplification coefficient with slope elevation under the excitation of an 8-Hz sine wave. Elevation exerts little influence. The seismic wave amplitude has a similar effect on the vertical PGA amplification factor as the horizontal direction pattern. Within a certain amplitude range (0.1–0.5 g), the amplification coefficient decreases with increasing amplitude. When the amplitude exceeds 0.5 g, the amplification coefficient increases with the increasing amplitude and then enters a downward trend. This reflects that with the accumulation of slope damage, the natural frequency decreases, the damping ratio increases (Xu et al. 2008), and the ability to resist deformation weakens.

Figure 13 shows the effect of the seismic wave frequency on the vertical PGA amplification coefficient. Similar to the horizontal PGA amplification coefficient, there is a frequency cutoff point.

Fig. 12 Effect of seismic wave amplitude on vertical PGA amplification coefficients at different elevations

Under the effect of different peak ground shaking at monitoring point A2, the vertical PGA amplification coefficient exhibits an inflection point at 10 Hz, indicating that the horizontal and vertical resonance curves are not the same, but both have non-resonant frequency ranges.

Failure mode analysis of the bedding rock slope

No significant deformation or failure occurred in model 1 after all loading conditions were completed. Model 2 was destroyed when the peak acceleration of the ground motion was 0.8 g. Model 3 was destroyed when the peak acceleration of the ground motion was 0.3 g. The joint strength parameters of model 2 were higher than those of model 3, and the energy required for failure was also higher.

Forward progressive failure mode

In model 2, cementing material C is used to simulate seismic working conditions. The slope generalization model diagram of the forward progressive failure mode is shown in Fig. 14, which marks the positions of the front edge, trailing edge, locking section, etc. The deformation and failure can be divided into four stages:

1. Initial creep-slide stage: At the beginning of the test, there is no obvious deformation on the slope surface, except partial loosening at the slope foot, as shown in Fig. 15a. This is because the slope body exhibits elastic deformation when the amplitude of the ground motion is small, and the strain energy gradually accumulates.

2. Crack extension stage: With the increase in the acceleration amplitude, the tension microcracks are generated at the trailing edge of the slope. These microcracks initiate at the weakest part depending on the dominant structural plane, and form stepped cracks. The stepped cracks perturb the seismic wavefield to induce secondary cracks to compete for propagation at the crack tip. Macroscopically, the displacement of the trailing edge is larger than that of the front edge, and the front edge forms multistage locking sections, controlling the initiation of
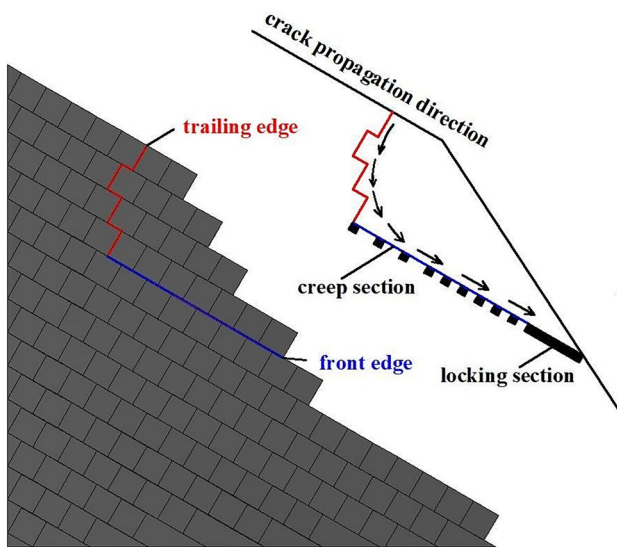
Fig. 14 Slope generalization model diagram of the forward progressive

the whole landslide, as shown in Fig. 15b. As the slope deformation increases, the stepped cracks grow and evolve under the action of the wave field, and the main cutting crack at the trailing edge of the slope extends to the tracking slip surface. The penetration of the sliding surface is blocked by the locking section, and the stress concentration at the locking section is strengthened (Huang et al. 2016; Dong et al. 2021). When the strain energy of the locking section reaches the limit, the locking section is cut step by step, the sliding belt is overlapped from the trailing edge to the front edge (Zou et al. 2012), and a hanging supporting shear outlet appears. In this process, the energy is continuously accumulated and transferred, eventually forming unstable slope structures.

3. Sudden departure stage: The cracks on the slope body continue to extend and propagate, and the sliding plane formed by the internal tracking joint surface of the rock body begins to penetrate, forming a potential slip surface. Under the combined action of the impact of the trailing edge wall of the slope and the friction accelerating effect of the sliding bed, not only

does the horizontal displacement of the sliding mass increase gradually, but the vertical displacement also obviously grows. A large amount of the strain energy accumulated by the locking section is released in a short time at the moment of cutting. It acts on the sliding mass separated from the sliding surface and is transformed into a rapid starting speed of the sliding mass. Then the sliding mass starts at a high speed and ejects toward the empty direction, as shown in Fig. 15c.

4. Final deceleration stage: The initiation velocity is superimposed on the sliding mass generated by the conversion of potential energy into kinetic energy, resulting in a high-speed stroke effect, as shown in Fig. 15d. With the friction effects such as collision, sliding, rolling, and viscosity, the energy of the ejected sliding mass is gradually dispersed and dissipated. When the sliding mass collides with the front baffle plate of the model box, the sliding mass rotates as a whole around its centroid. Broken sliders are embedded in the wedge-shaped space formed by the slope surface and the baffle plate of the model box, and the landslide motion is terminated. The stepped failure surface of the Layue landslide forms from the stepped slide bed and the nearly vertical steep wall at the trailing edge of the slope shoulder. This pattern reproduces that before the occurrence of the Layue landslide and exhibits the development process of surface crack deepening and widening caused by successive cumulative earthquakes, as well as several small collapses of the rolling stones.

Backward progressive failure mode

In model 3, cementing material D was used to simulate the working conditions of earthquakes and rainfall. The slope generalization model diagram of the backward progressive failure mode is shown in Fig. 16. The deformation and failure can be divided into four stages:

1. Initial creep-slide stage: The strength parameters of the structural plane are further attenuated due to rainfall infiltration. When the amplitude of the ground motion is small, there is no significant displacement or deformation of the slope body, as shown in Fig. 17a.
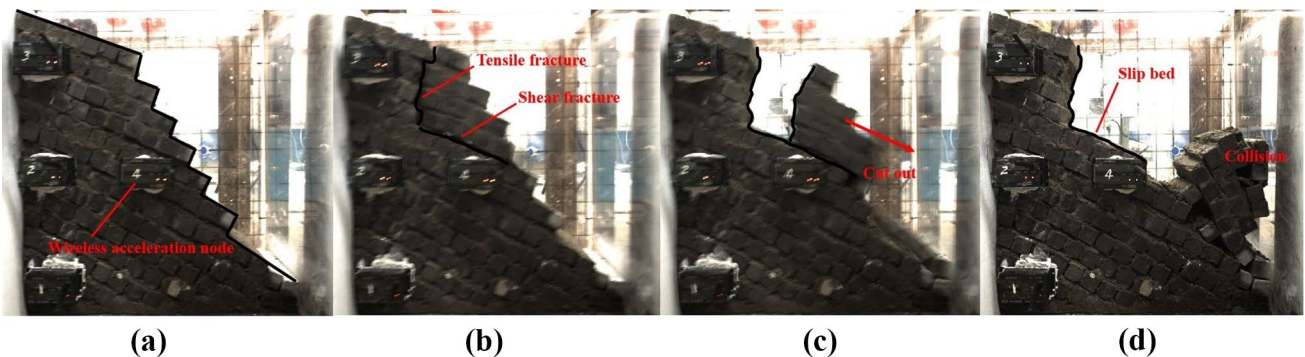
Fig. 15 Forward progressive failure mode: **a** initial creep-slip stage; **b** crack extension stage; **c** sudden departure stage; **d** final deceleration stage

Fig. 16 Slope generalization model diagram of the backward progressive failure mode
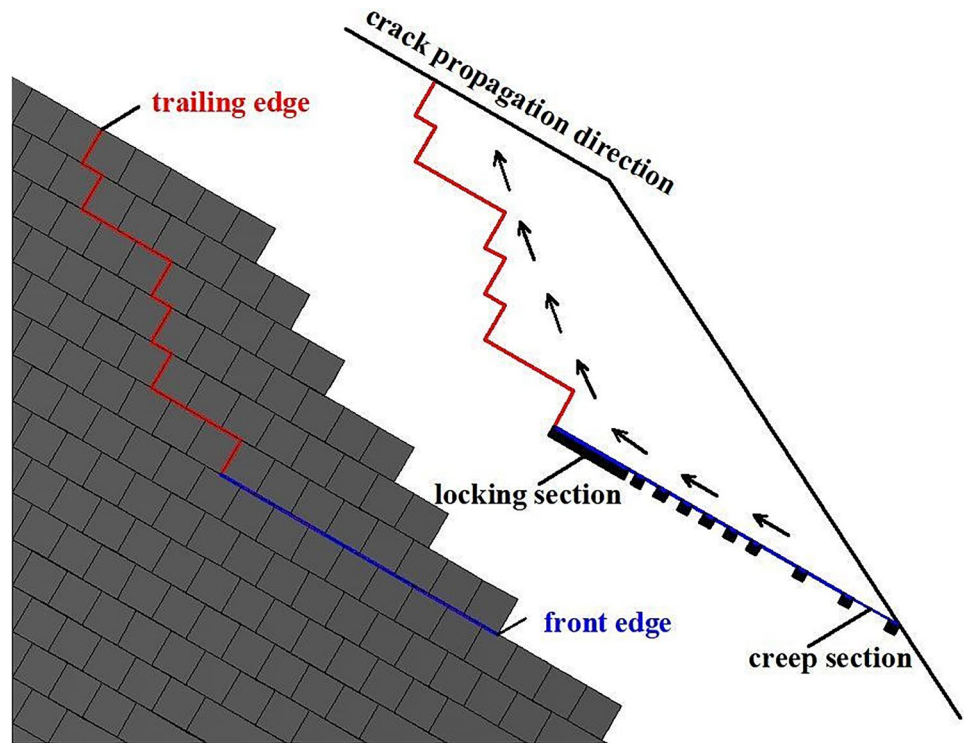
2. Crack extension stage: As shown in Fig. 17b, with the increase in the acceleration amplitude, the creep section at the front edge of the slope is obliquely cut through and penetrated, and the displacement is large at the front edge, and the displacement is small at the trailing edge. Macroscopically expressed as the trailing edge forming multistage locking sections, the trailing edge of the landslide controls the initiation of the whole landslide. The rock block near the foot of the slope tipped over, and two types of cracks appeared on the slope. The first type is the main crack formed by the extension of the overturned rock mass along the interlayer joints and secondary joints to the shoulder of the slope. The sliding mass moves along the main crack as a whole. The other type is secondary stepped tension cracks formed relying on conjugate joint planes, which are arranged in parallel echelons in the front and back. With the continuous input of ground motion energy, the main cut-

ting cracks extend to the locking section of the trailing edge, and the locking section experiences stress accumulation and step-by-step shear. The sliding surface tracks upward along the conjugate joint plane and spreads out in a step shape, finally forming an unstable slope structure.

3. Overall collapse stage: With the sliding belt from the front and trailing edges gradually lapped, the stability of the slope was broken. This caused the collapse failure and continuous sliding of the chimeric massive rock mass in the whole slope, forming an overall large-scale landslide, as shown in Fig. 17c. The sliders in front of the secondary cracks first fall to the foot of the slope. The main cracks and microcracks in the slope gradually evolve into cavities in the process of collapse. Therefore, the upper slide body loses support and sinks in, then disintegrates and breaks continuously.

4. Tipping and stacking stage: The sliding mass collides and scrapes with the base material. This creates a debris flow between "fluid"
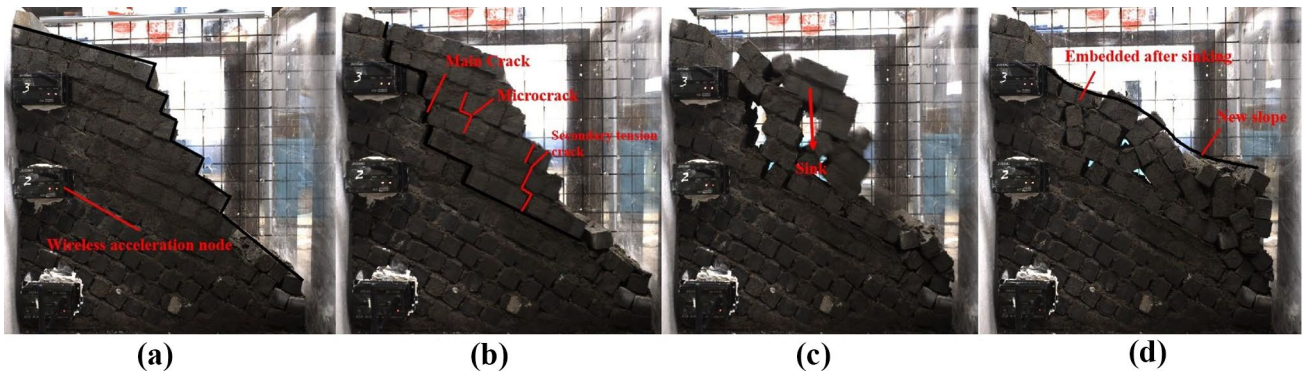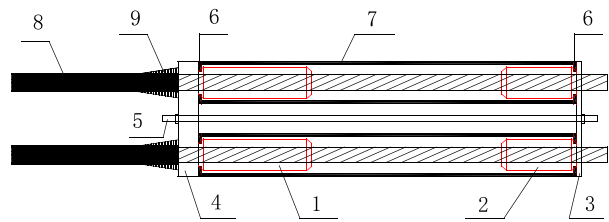

Fig. 17 Backward progressive failure mode: **a** initial creep-slip stage; **b** crack extension stage; **c** overall collapse stage; **d** tipping and stacking stage

(a)

(b)

Fig. 18 Design scheme of seismic anchor cable: **a** seismic anchor cable; **b** adaptive regulator: 1—seismic anchor; 2—permanent anchors; 3—fastening plate; 4—carrier; 5—fastening screw; 6—rubber pad; 7—sealing cover; 8—unbonded steel strand; 9—sealing tape

and "bulk" under the slipstream motion state, overturning and accumulating at the intersection angle between the slope foot and baffle plate of the model box, as shown in Fig. 17d. After the landslide movement stops, due to the scraping of the sliding rock mass and the downslope accumulation of lower rock blocks, a relatively steep slope with a slope gradient between 35 and 40° is formed, and the slope angle reaches a stable state of the natural angle of repose. This kind of failure mode and accumulation mode of the sliding mass reproduced the phenomenon observed for the Layue landslide, which gradually disintegrates and develops into a debris flow. It often appears on the side slope of the valley zone where rock mass joints and cracks are developed. The V-shaped valley of the Layue landslide creates good topographic conditions for its unstable sliding.

Seismic anchor cable reinforcement of bedding rock slope
A strong earthquake may cause the forward and backward progressive failure of the slope, causing great harm. Under the condition of a strong earthquake, due to the large deformation of the anchorage rock mass, it is generally difficult for the conventional anchor cable to continue to limit its deformation. At this time, the anchor cable is easily pulled out due to the insufficient deformation capacity of the anchor cable or the overload under the instantaneous impact load. Therefore, it is necessary to optimize the conventional anchor cable system from the perspective of material and structure, so that the deformation of the anchor cable is coordinated with that of the rock and soil mass.

The seismic anchor cable (Fig. 18) is based on a pressure-type anchor cable. Its special adaptive device can buffer the seismic instantaneous seismic wallop. According to the load size or rock mass deformation, deformation adjusts itself to adapt to the substantial deformation of the rock and soil body. The cable could maintain constant tension, avoid anchoring system overload or damage, and achieve the goal of large deformation or surrounding rock slope reinforcement. This is suitable for high seismic intensity, blasting and vibration environments and large deformation, and large-section geotechnical reinforcement engineering.

The basic structure of the seismic anchor cable is shown in Fig. 18. The anchor cable comprises a free section and an anchor section, and the anchor section is installed with a seismic anchoring device (Xu et al. 2018). The anchor cable passes through the bearing plate, seismic anchor, and permanent anchor in turn. The seismic anchor is a sliding extruded sleeve structure with maximum anchoring force, which is pressed inside the bearing plate under static load. The permanent anchors are standard extruded sleeves and cannot slip. The inertial force of the downhill body under seismic load rapidly increases the anchor cable's stress. When the instantaneous impact force is greater than the maximum static friction force between the seismic anchor and the anchor cable, the relative yield slip between the anchor and the seismic anchor is triggered (point A in Fig. 19). The free section of the anchor cable is extended to reduce the instantaneous impact force of the earthquake and avoid the overload of the anchor system. When the seismic wave energy is further accumulated, the bond between the
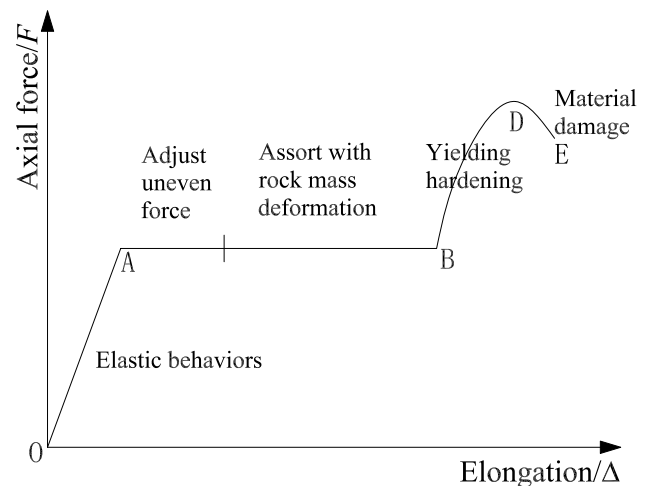
Fig. 19 Axial force–elongation relation of seismic anchor cable

anchor cable and seismic anchor continues to slip until the reserved slip amount (distance between the seismic anchor and permanent anchor, point B in Fig. 19) is exhausted. The energy released by rock mass deformation is absorbed and dissipated mainly through the yield slip of the anchor cable, and less energy is absorbed through the deformation of the anchor cable itself. The seismic anchor cable can coordinate with the large deformation of the rock mass due to the existence of its unique adaptive yielding device, which can better solve the problems faced by the traditional type of anchor cable.

Conclusions

1. The seismic characteristics and geological structure of the slope are two basic determinants that jointly determine the seismic dynamic stability and failure mode of the slope. Due to the different triggering factors and geological conditions, bedding rock landslides often exhibit different energy storage mechanisms and energy release mechanisms. These significantly determine different slope deformation and instability development and evolution processes.

2. The horizontal dynamic response of the slope has an obvious elevation amplification effect and topographic effect. The amplification effect of a sine wave on the horizontal acceleration of the slope is more significant than that of a natural wave. The effects of the seismic amplitude and mechanical parameters of slope bedding joints on horizontal PGA amplification coefficient both have an inflection point at 0.3 g peak ground motion acceleration. The slope has multi-order natural frequencies, and the inherent frequency is time-varying under seismic loading.

3. Elevation has little effect on the vertical dynamic response of the slope. The seismic wave amplitude has a similar effect on the vertical PGA amplification coefficient as the horizontal direction pattern, and there is an amplitude interval with 0.5 g as the cutoff point. The seismic wave spectrum has a significant effect on the dynamic response in both the horizontal and vertical directions.

4. The joint planes of the restrained sliding mass are simultaneously subjected to the coupling effects of dynamic shear and tension. If the mechanical properties of the joint surface are strong, tensile microcracks appear at the trailing edge of the slope first, and the displacement of the trailing edge is larger than that of the front edge. The slide zone is lapped from the front edge to the trailing edge (forward progressive failure), and the implicated slide block is cut out at a high position as a whole, forming a steep wall and step-like slide bed at the trailing edge. If the joints are weakened by external geological forces, the creep section of the front edge is first to cut through diagonally, and the displacement of the front edge is large, while the displacement of the trailing edge is small. The slip belt is lapped from the front to trailing edges (backward progressive failure), which pulls the chimeric massive rock mass in the whole slope body to collapse and form debris flows in the sliding flow state.

5. The seismic anchor cable uses the mechanical sliding mechanism under strong earthquake conditions. This has many effects: for example, buffering the transient impact of the earthquake, regulating the uneven force of the anchor cable, coordinating the deformation of the geotechnical body, and reducing the risk of the anchor cable being pulled off or displaced, thus avoiding the overall damage to the anchorage system, guaranteeing the safety and stability of the slope and improving the safety reserve of the anchorage structure.

Author contribution

Conceptualization and methodology, M.X.; software and validation, X.Y.Y. and Y.H.P.; formal analysis, X.S.L.; investigation and resources, Y.P.Z. and J.J.H. All authors have read and agreed to the published version of the manuscript.

Data availability

Seismic data was obtained from Information Management System for Strong Earthquake Ground Motion developed by Dong YF, Yang P, Li YM, and Zheng NN (Software Copyright, RN2016SR284893). The calibration of the seismic wave was performed using SeismoSignal 5.1.2, developed by the SeismoSoft Company.

Declarations

Conflict of interest   The authors declare no competing interests.

References

Chen XQ, Cui P, Li Y, Zhao WY (2011) Emergency response to the Tangjiashan landslide dammed lake resulting from the 2008 Wenchuan earthquake, China. Landslide 8(1):91–98. https://doi.org/10.1007/s10346-010-0236-6

Deng QH, Gong LX, Zhang LP, Yuan RM, Xue YQ, Geng XK, Hu SX (2017) Simulating dynamic processes and hypermobility mechanisms of the Wenjiagou rock avalanche triggered by the 2008 Wenchuan earthquake using discrete element modelling. Bull Eng Geol Env 76:923–936. https://doi.org/10.1007/s10064-016-0914-2

Dong JY, Wang C, Huang ZQ et al (2022) Shaking table model test to determine dynamic response characteristics and failure modes of steep bedding rock slope. Rock Mech Rock Eng 55(10):3645–3658. https://doi.org/10.1007/s00603-022-02822-x

Dong JY, Wang C, Huang ZQ, Yang JH, Xue L (2021) Dynamic response characteristics and instability criteria of a slope with a middle locked segment. Soil Dyn Earthq Eng 150:106889. https://doi.org/10.1016/j.soildyn.2021.106899

Eberhardt E, Stead D, Coggan J (2004) Numerical analysis of initiation and progressive failure in natural rock slopes—the 1991 Randa rockslide. Int J Rock Mech Min Sci 41(1):69–87. https://doi.org/10.1016/S1365-1609(03)00076-5

Fan G, Zhang JJ, Wu JB et al (2016) Dynamic response and dynamic failure mode of a weak intercalated rock slope using a shaking table. Rock Mech Rock Eng 49(8):3243–3256. https://doi.org/10.1007/s00603-016-0971-7

Feng XX, Jiang QH, Zhang XB et al (2019) Shaking table model test on the dynamic response of anti-dip rock slope. Geotech Geol Eng 20(02):242–248

Gischig VS, Eberhardt E, Moore JR, Hungr O (2015a) On the seismic response of deep-seated rock slope instabilities—insights from numerical modeling. Eng Geol 193(2):1–18. https://doi.org/10.1016/j.enggeo.2015.04.003

Gischig V, Preisig G, Eberhardt E (2015b) Numerical investigation of seismically induced rock mass fatigue as a mechanism contributing to the progressive failure of deep-seated landslides. Rock Mech Rock Eng 49(6):2457–2478. https://doi.org/10.1007/s00603-015-0821-z

He JX, Qi SW, Zhan ZF et al (2021) Seismic response characteristics and deformation evolution of the bedding rock slope using a large-scale shaking table. Landslides 18(8):2835–2853. https://doi.org/10.1007/s10346-021-01682-w

Hovius N, Meunier P (2012) Earthquake ground motion and patterns of seismically induced landsliding. In: Clague J, Stead D (eds) Landslides: types, mechanisms and modeling. Cambridge University Press, Cambridge, 3:24–36. https://doi.org/10.1017/CBO9780511740367.004

Huang RQ, Li WL (2009) Analysis of the geo-hazards triggered by the 12 May 2008 Wenchuan earthquake, China. Bull Eng Geol Env 68(3):363–371. https://doi.org/10.1007/s10064-009-0207-0

Huang RQ, Xu Q, Huo JJ (2011) Mechanism and geo-mechanics models of landslides triggered by 5.12 Wenchuan earthquake. J Mt Sci 8(2):200–210. https://doi.org/10.1007/s11629-011-2104-9

Huang RQ, Chen GQ, Tang P (2017) Precursor information of locking segment landslides based on transient characteristics. Chin J Rock Mech Eng 36(03):521–533. https://doi.org/10.13722/j.cnki.jrme.2016.1100 (in Chinese)

Li K, Wang YF, Lin QW et al (2021) Experiments on granular flow behavior and deposit characteristics: implications for rock avalanche kinematics. Landslides 18:1779–1799. https://doi.org/10.1007/s10346-020-01607-z

Liang QG, Han WF, Ma RY et al (2005) Physical simulation study on dynamic failures of layered rock masses under strong ground motion. Rock Soil Mech 26(8):1307–1311. https://doi.org/10.16285/j.rsm.2005.08.026

Liu H, Qiu T, Xu Q (2021a) Dynamic acceleration response of a rock slope with a horizontal weak interlayer in shaking table tests. Public Library of Science 16(4):e0250418. https://doi.org/10.1371/journal.pone.0250418

Liu HD, Zhao YW, Dong JY et al (2021b) Experimental study of the dynamic response and failure mode of anti-dip rock slopes. Bull Eng Geol Env 80(8):6583–6596. https://doi.org/10.1007/s10064-021-02313-3

Liu HX, Xu Q, Li YR, Fan XM (2013) Response of high-strength rock slope to seismic waves in a shaking table test. Bull Seismol Soc Am 103(6):3012–3025. https://doi.org/10.1785/0120130055

Huang RQ, Chen GQ, Guo F, Zhang GF, Zhang Y (2016) Experimental study on the brittle failure of the locking section in a large-scale rock slide. Landslides 13(3):583–588. https://doi.org/10.1007/s10346-015-0673-3

Sassa K, Nagai O, Solidum R, Yamazaki Y, Ohta H (2010) An integrated model simulating the initiation and motion of earthquake and rain induced rapid landslides and its application to the 2006 Leyte landslide. Landslides 7:219–236. https://doi.org/10.1007/s10346-010-0230-z

Tao ZG, Ren SL, Hao Y et al (2021) Physical model experiment on failure mechanism and NPR anchor cable control effect of layered counter-tilt slope. Rock Soil Mech 42(04):976–990. https://doi.org/10.16285/j.rsm.2020.0384

Wang G, Du CY, Huang DR et al (2018) Parametric models for 3D topographic amplification of ground motions considering subsurface soils. Soil Dyn Earthq Eng 115(Dec.):41–54. https://doi.org/10.1016/j.soildyn.2018.07.018

Wang LF, Zhou XP (2021) A field-enriched finite element method for simulating the failure process of rocks with different defects. Comput Struct 250:1–23. https://doi.org/10.1016/j.compstruc.2021.106539

Xu GX, Yao LK, Gao ZN et al (2008) Large-scale shaking table model test study on dynamic characteristic and dynamic response of slope. Chin J Rock Mech Eng 27(03):624–624 (in Chinese)

Xu M, Tang YF, Liu XS et al (2018) A shaking table model test on a rock slope anchored with adaptive anchor cables. Int J Rock Mech Min Sci 112:201–208. https://doi.org/10.1016/j.ijrmms.2018.10.021

Yang GX, Qi SW, Wu FQ et al (2018) Seismic amplification of the anti-dip rock slope and deformation characteristics: a large-scale shaking table test. Soil Dyn Earthq Eng 115:907–916. https://doi.org/10.1016/j.soildyn.2017.09.010

Ye HL, Zheng YR, Du XL et al (2012) Shaking table model test and numerical analysis on dynamic failure characteristics of slope. Chin Civ Eng J 45(09):128–135. https://doi.org/10.15951/j.tmgcxb.2012.09.002 (in Chinese)

Yin YP, Wang FW, Sun P (2009) Landslide hazards triggered by the 2008 Wenchuan earthquake, Sichuan, China. Landslides 6(2):139–152. https://doi.org/10.1007/s10346-009-0148-5

Zhang M, Yin YP, Wu SR, Zhang YS, Han JL (2011) Dynamics of the Niumiangou Creek rock avalanche triggered by 2008 Ms 8.0 Wenchuan earthquake, Sichuan, China. Landslides 8:363–371. https://doi.org/10.1007/s10346-011-0265-9

Zhou JW, Cui P, Fang H (2013) Dynamic process analysis for the formation of Yangjiagou landslide-dammed lake triggered by the Wenchuan earthquake, China. Landslides 10:331–342. https://doi.org/10.1007/s10346-013-0387-3

Zhou XP, Jia ZM, Wang LF (2021) A field-enriched finite element method for brittle fracture in rocks subjected to mixed mode loading. Eng Anal Boundary Elem 129(1):105–124. https://doi.org/10.1016/j.enganabound.2021.04.023

Zou ZX, Tang HM, Xiong CR et al (2012) Geo-mechanical model of progressive failure for large consequent bedding rock slide and its stability analysis. Chin J Rock Mech Eng 31(11):2222–2230

Ming Xu (✉) · Xiaoyue Yu · Yuhua Pan · Xianshan Liu
Faculty of Civil Engineering, Chongqing University, Chongqing 400045, China
Email: foretech@163.com

Xiaoyue Yu
Email: sweetmoonlet@163.com

Ming Xu · Xianshan Liu
National Joint Engineering Research Center of Geohazards Prevention in the Reservoir Areas, Chongqing University, Chongqing 400045, China

Yuanping Zhao
CISDI Engineering Co., Ltd., Chongqing 400013, China

Jiaju Hu
China Construction Fifth Engineering Division Corp., Ltd., Changsha 410004, China